Liquid Crystals
Publication details, including instructions for authors and subscription information:
http://www.informaworld.com/smpp/title~content=t713926090

Switching of chirality from racemic to homochiral state in new liquid crystalline monomers with bent-core molecules

Vladimíra Novotná[a]; Věra Hamplová[a]; Miroslav Kašpar[a]; Milada Glogarová[a]; Damian Pociecha[b]
[a] Institute of Physics, Academy of Sciences of the Czech Republic, 182 21 Prague 8, Czech Republic [b] Laboratory of Dielectrics and Magnetics, Chemistry Department, Warsaw University, 02-089 Warsaw, Poland

To cite this Article Novotná, Vladimíra , Hamplová, Věra , Kašpar, Miroslav , Glogarová, Milada and Pociecha, Damian(2005) 'Switching of chirality from racemic to homochiral state in new liquid crystalline monomers with bent-core molecules', Liquid Crystals, 32: 9, 1115 — 1123
To link to this Article: DOI: 10.1080/02678290500303270
URL: http://dx.doi.org/10.1080/02678290500303270

Liquid Crystals, Vol. 32, No. 9, September 2005, 1115–1123

Switching of chirality from racemic to homochiral state in new liquid crystalline monomers with bent-core molecules

VLADIMÍRA NOVOTNÁ*†, VĚRA HAMPLOVÁ†, MIROSLAV KAŠPAR†, MILADA GLOGAROVÁ† and DAMIAN POCIECHA‡

†Institute of Physics, Academy of Sciences of the Czech Republic, Na Slovance 2, 182 21 Prague 8, Czech Republic
‡Laboratory of Dielectrics and Magnetics, Chemistry Department, Warsaw University, Al. Zwirki i Wigury 101, 02-089 Warsaw, Poland

(*Received 20 April 2005; accepted 25 June 2005*)

The synthesis and physical properties of bent-shaped molecules with ester linkages and methoxy substitution on a non-central ring are presented. Terminal chains of most mesogens contain a group with double bond, which promotes polymerization. In all the compounds studied a B_2 phase just below the isotropic phase has been found. Polarization current profiles indicate that this phase is antiferroelectric, and dielectric spectroscopy data with a pronounced high frequency mode support this fact. For several compound chirality switching from racemic to the homochiral state was seen after application of a low frequency a.c. field. Another phase, which could be assigned to the B_7 family, appears below the B_2 phase on cooling.

1. Introduction

Liquid crystalline mesophases formed by bent-core (banana-shaped) mesogens have attracted particular interest since their first observation [1]. The B_2 phase, which exhibits electro-optic switching, is the most studied banana mesophase. In this phase the molecules are packed in layers and tilted from the layer normal [2, 3]. The B_2 phase exhibits polar properties, mostly antiferroelectric [4–6] with only a few ferroelectric exceptions [7–10], resulting from hindered molecular rotation around the molecular long axis. The packing of bent-shaped molecules in smectic layers creates structural layer chirality even though the molecules are non-chiral. As both layer chiralities are possible for one compound, both racemic and homochiral structures can be created. Thus, two distinct antiferroelectric B_2 phase structures have been proposed, racemic SmC_SP_A and chiral SmC_AP_A, synclinic and anticlinic in molecular tilt in adjacent layers, respectively [2].

Besides the B_2 phase, much effort has been devoted to the B_7 phase, which exhibits unusual textures. On the base of synchrotron X-ray, freeze fracture and optical investigation, a structural model with commensurable one-dimensional undulation has been proposed [11]. This phase does not exhibit in-plane order like the B_2 phase, and its electro-optic switching is very limited probably due to large threshold fields.

Here we suggest the possibility of creating polymers based on bent-core monomers, which can combine the unique properties of polymers and those of liquid crystalline compounds, and thus offer new applications potential. So far only a few polymers have been reported based on bent-core mesogens [12]. We now present a series of mesogens with bent-core molecules possessing a polymerizable group at one or both ends of the terminal alkyl chain. The new compounds are derived from a symmetrical bent molecular core with a methoxy group laterally substituted on the rings next to the central ring. Recently, the same core has been used for compounds exhibiting two mesophases. The high temperature phase denoted as the B_H phase has been established as the SmC_SP_A phase [13]. On the basis of synchrotron studies the low temperature phase lying below the B_2 phase on cooling (in [13] denoted as the B_L phase) has been confirmed as a typical B_7 phase [14]. We have now studied the mesomorphic properties of new monomeric compounds prepared for the further synthesis of polymers.

2. Synthesis

The synthesis of new bent-shaped mesogenes (see scheme 1) was carried out according to the process of scheme 2. The preparation of mesogenic phenol **M1** has

*Corresponding author. Email: novotna@fzu.cz

Liquid Crystals
ISSN 0267-8292 print/ISSN 1366-5855 online © 2005 Taylor & Francis
http://www.tandf.co.uk/journals
DOI: 10.1080/02678290500303270

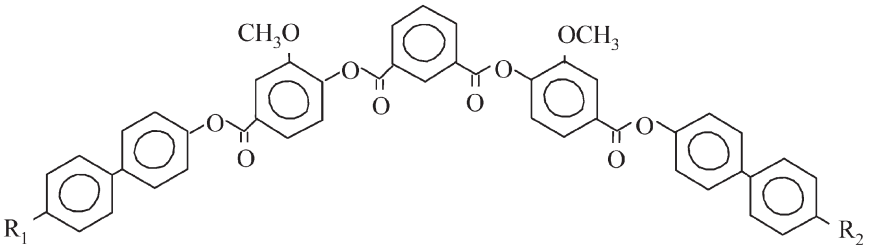

$R_1, R_2 = -OC_nH_{2n+1}, -C_nH_{2n+1}, -OC_9H_{18}CH{=}CH_2$

Scheme 1. Chemical structure of studied bent-shaped molecules.

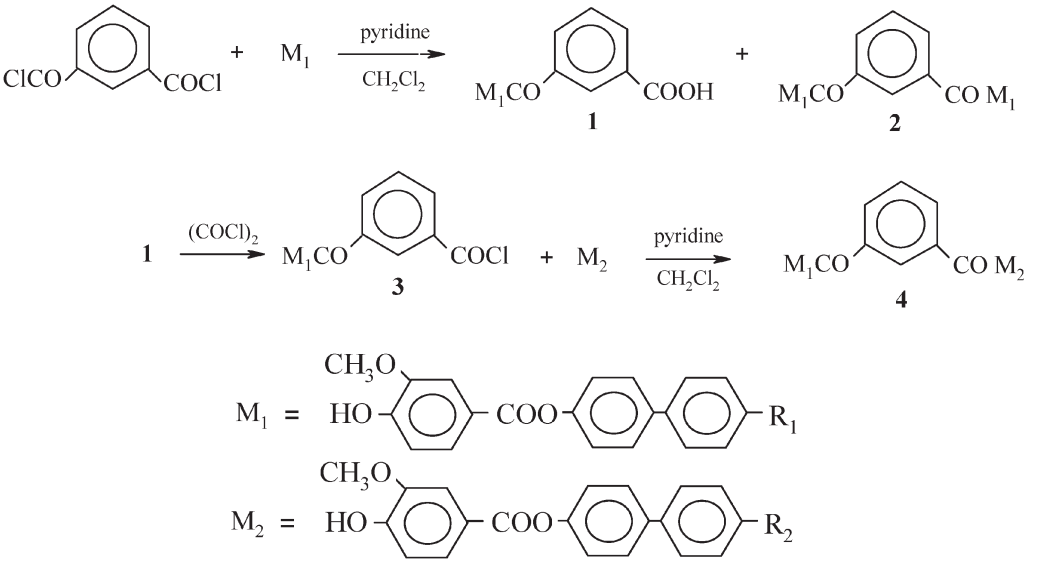

Scheme 2. Synthesis route.

previously been described in detail [13]. The intermediates and final products were purified, and their molecular structures confirmed by NMR analysis.

2.1. *Mesogenic acids,* 1

The mesogenic acids **1** were obtained by esterification of mesogenic phenols $\mathbf{M_1}$ (20 mmol) with 15 g of isophthaloyl chloride in dichloromethane/pyridine solution. The reaction mixture was heated under reflux for 4 h and held at room temperature overnight. Then 50 ml of dioxane and 10 ml of water were added and the mixture stirred for 1 h at room temperature. The mixture was washed with dilute HCl and the excess of unreacted isophthalic acid separated by filtration. The filtrate was washed with water and the solvent evaporated. The solid residue was crystallized from glacial acetic acid; the crystalline precipitate contained a small amount of symmetrical product **2**. Further purification was carried out by recrystallization from ethanol in which symmetrical product **2** is more soluble then acid **1**. Compound **1** ($R_1{=}OC_{10}H_{21}$), 1H NMR: 8.97 s (1H, HAr between –COO in isoph.acid); 8.4 dd (2H, HAr *ortho* to –COO in isoph. acid); 7.95 d (1H, HAr *para* to $-OCH_3$); 7.4–7.7m (1H, HAr *meta* to –COO in isoph.acid+4H HAr *ortho* to –Ar); 7.3 m (3H, HAr *ortho* to –OCO); 6.97 d (2H, HAr *ortho* to $-OCH_2$); 4.0 t (4H, CH_2OAr) 3.95 s (3H, $-OCH_3$); 1.8 quint (2H, $\underline{CH_2}CH_2OAr$); 1.2–1.6 m (14H, CH_2); 0.9 t (3H, CH_3).

2.2. *Acyl chloride,* 3

The mesogenic acids **1** were converted into corresponding acyl chlorides **3** by refluxing the dry acids with an excess of oxalyl chloride overnight. Excess oxalyl chloride was distilled off *in vacuo*, the residue dissolved

in dichloromethane and filtered, and the solution used for esterification of mesogenic phenol $\mathbf{M_1}$ using standard reaction conditions. Compound **3** (R_1=$OC_{10}H_{21}$), 1H NMR: 8.98 s (1H, HAr between –COO and COCl); 8.56 d (1H, HAr *ortho* to –COCl); 8.40 d (1H, HAr *ortho* to –COO); 7.95 d (1H, HAr *para* to $-OCH_3$); 7.7 t (1H, HAr *meta* to –COCl); 7.5 and 7.6 dd (4H, HAr *ortho* to –Ar); 7.3 m (3H, HAr *ortho* to –OCO); 7.0 d (2H, HAr *ortho* to $-OCH_2$); 4.0 t (4H, CH_2OAr); 3.95 s (3H, $-OCH_3$); 1.8 quint (2H, CH_2CH_2OAr); 1.2–1.6 m (14H, CH_2); 0.9 t (3H, CH_3).

2.3. *Preparation of mesogenic phenol,* $\mathbf{M_2}$

The preparation of unsaturated mesogenic phenol $\mathbf{M_2}$ (R_2=$-OC_9H_{18}CH{=}CH_2$) was carried out as in [13], using 10-undecyl bromide as starting material. Mesogenic phenol $\mathbf{M_2}$ with R_2=$-C_{10}H_{21}$ was prepared by Friedel–Crafts acylation of 4-acetyloxybiphenyl and subsequent redesction of the keto group in zinc/hydrochloride acid mixture [15].

2.4. *Preparation of final products* 4a–e

Final products were prepared by esterification in pyridine/dichloromethane mixture using standard reaction conditions. The crude products were crystallized twice from toluene/acetone and toluene/methanol mixtures, and purified by column chromatography on silica gel using a mixture of dichloromethane and acetone (99.5/0.5) as eluant. The structure of all final products **4a**–**e** was confirmed by ^{1}H NMR (200 MHz, $CDCl_3$, Varian, Gemini 2000). Chemical purity was checked by high pressure liquid chromatography (HPLC), which was carried out with an Ecom HPLC chromatograph using a silica gel column (Separon 7 μm, 3 × 150, Tessek) and toluene/methanol (99.9/0.1) as eluant, with detection of the eluting products by a UV-Vis detector (λ=290 nm). The chemical purity was found to be 99.9% under these conditions. Compound **4b** (R_1=$-OC_{10}H_{21}$, R_2=$-OC_9H_{18}CH{=}CH_2$), 1H NMR: 9.1 s (1H, HAr between –COO in isoph.acid); 8.5d (2H, HAr *ortho* to −COO in isoph.acid); 7.95 d (2H, HAr *para* to $-OCH_3$); 7.88 s (2H, HAr *ortho* to $-OCH_3$); 7.75 t (1H, HAr *meta* to –COO in isoph.acid); 7.5–7.65 m (8H, HAr ortho to −Ar); 7.3 m (6H, HAr ortho to –OCO); 6.98 d (4H, HAr *ortho* to $-OCH_2$); 5.8 m (1H, C=CH–); 5.0 m (2H, CH_2=C); 4.0 t (4H, CH_2OAr); 3.94 s (6H, $-OCH_3$); 2.05 q (2H, CH_2=CH–$\underline{CH_2}$); 1.8 m (4H, $\underline{CH_2}$–CH_2–OAr); 1.3–1.6 m (26H, CH_2); 0.9 t (3H, CH_3). Compound **4d** (R_1=$-C_{10}H_{21}$, R_2=$-OC_{10}H_{21}$), 1H NMR: 9.1 s (1H, HAr between –COO in isoph. acid); 8,5 d (2H, HAr *ortho* to –COO in isoph. acid); 7.95d (2H, HAr *para* to $-OCH_3$); 7.88 s (2H, HAr *ortho* to $-OCH_3$); 7.75 t (1H, HAr *meta* to –COO in isoph. acid); 7.5–7.7 m (8H, HAr *ortho* to Ar); 7.2–7.4 m (6H, HAr *ortho* to –OCO and 2H, HAr *ortho* to $-CH_2$); 6.98 d (2H, HAr *ortho* to $-CH_2$); 4.0 t (2H, CH_2OAr); 3.94s (6H, $-OCH_3$); 2.65 t (2H, $-CH_2Ar$); 1.2–1.8 m (32H, CH_2); 0.90 t (6H, CH_3).

3. Experimental

DSC studies were performed using a Perkin–Elmer (Pyris Diamond) calorimeter, with cooling and heating rates of 5 K min^{-1}. The samples were placed in aluminium pans hermetically closed under nitrogen. The samples for electro-optical measurements were filled in the isotropic phase into cells composed of glass plates provided with ITO electrodes. The sample thickness (usually 3.5 or 6 μm) was defined by mylar sheets. Free-standing films were prepared by spreading the materials across a hole in a metallic plate. A polarizing microscope (Nikon Eclipse E-600) equipped with a hot stage (Linkam TMS 94) was used. Temperature was changed and stabilized with an accuracy of $\pm$0.1°C.

Switching properties were studied under an electrical voltage up to 150 V. A memory oscilloscope leCroy 9304 provided the switching current profile versus time. Dielectric properties were studied using a Schlumberger 1260 impedance analyser. Frequency dispersions were measured in the range 10 Hz–1 MHz on cooling at a rate of about 0.2 K min^{-1}, keeping the temperature of the sample stable during frequency sweeps. The frequency dispersion data were analysed using the Cole–Cole formula for the frequency-dependent complex permittivity $\varepsilon^*(f)=\varepsilon' - i\varepsilon''$:

$$\varepsilon^* - \varepsilon_\infty = \frac{\Delta\varepsilon}{1+(if/f_r)^{(1-\alpha)}} - i\frac{\sigma}{2\pi\varepsilon_0 f^n} + Af^m \qquad (1)$$

where f_r is the relaxation frequency, $\Delta\varepsilon$ is the dielectric strength, α is the distribution parameter, ε_0 is the permittivity of a vacuum, ε_∞ is the high frequency permittivity and n, m, A are parameters of fitting. The second and third terms in the equation are used to eliminate a low frequency contribution from d.c. conductivity σ and a high frequency contribution due to resistance of the ITO electrodes, respectively.

X-ray studies were performed using a DRON system equipped with Ge monochromator. Experiments were conducted on non-oriented samples in the reflection mode.

4. Results

4.1. *DSC study*

In DSC measurements two mesophases were detected in all the materials studied. The phase transition temperatures and enthalpies evaluated from DSC plots are

Table 1. Melting points (m.p.), transition temperatures and transition enthalpies (in square brackets) taken on cooling from the isotropic phase. R_n indicates the type of alkyl or alkoxy chain (see scheme 1).

Compound	R_1	R_2	m.p./°C [ΔH/J g^{-1}]	T_{cr}/°C [ΔH/J g^{-1}]	B_7	T/°C [ΔH/J g^{-1}]	B_2	T/°C [ΔH/J g^{-1}]	I
4a	$-OC_8H_{17}$	$-OC_9H_{18}CH=CH_2$	164 [+26.8]	148 [−24.3]	•	200 [−1.1]	•	205 [−22.7]	•
4b	$-OC_{10}H_{21}$	$-OC_9H_{18}CH=CH_2$	148 [+33.8]	107 [−16.2]	•	165 [−0.58]	•	205 [−22.3]	•
4c	$-OC_{11}H_{23}$	$-OC_9H_{18}CH=CH_2$	144 [+31.9]	125 [−16.5]	•	155 [−0.43]	•	207 [−20.3]	•
4d	$-OC_9H_{18}CH=CH_2$	$-OC_9H_{18}CH=CH_2$	140 [+17.6]	121 [−15.3]	•	153 [−0.47]	•	198 [−19.4]	•
4e	$-OC_{10}H_{21}$	$-C_{10}H_{21}$	148 [+25.4]	121 [−15.2]	•	146 [−0.38]	•	204 [−16.9]	•

summarized in table 1. Two typical profiles of DSC plots corresponding to second heating and cooling runs are shown in figures 1 (*a*) and 1 (*b*) for compounds **4c** and **4d**, respectively. In figure 1 (*b*) for **4d**, an opposing broad peak is seen in the thermogram taken on heating. This anomaly persists even on cooling the compound to≈−25°C before subsequent heating, and could be explain by a partial recrystallization. In the inset of figure 1 (*a*), the thermogram profile in the vicinity of the phase transition between mesophases is shown in enlarged scale. The enthalpy change for this phase transition is relatively small, in the range 0.4–1.1 J g^{-1} (table 1).

4.2. *Texture observations*

In planar geometry the high temperature phase exhibits a fan-shaped texture typical for the B_2 phase. Usually stripes parallel to the smectic layers appear on cooling from the isotropic phase, see figure 2 (*a*) for compound **4b**. Stripes parallel to the directions of the light polarization are in the optical extinction. Using an optical compensator we found the long axis of optical indicatrix is parallel to the smectic layer normal. On further cooling, transition from the B_2 phase to a low temperature phase takes place. Birefringence and the texture character change, and additional defects appear, see figure 2 (*b*). The low temperature phase is identified as the B_7 phase (see below).

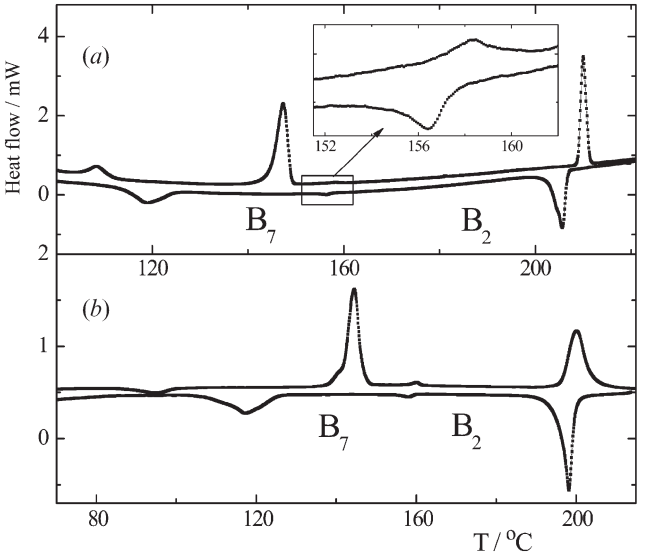

Figure 1. Typical DSC plots for compounds (*a*) **4c** and (*b*) **4d**. The upper and lower curves show second heating and cooling runs, respectively. The rectangle indicates indistinct phase transitions, which are seen in enlarged view in the inset. The slopes are adjusted for convenience.

For all the compounds studied, free-standing films were prepared at temperatures several degrees below the transition to the isotropic phase. The films persist during further heating and observation of the transition from the isotropic to the B_2 phase is possible. A schlieren texture is found in free-standing films of the B_2 phase, which indicates a full degeneracy of the director in-plane orientation. In figure 3 (*a*) the transition from the isotropic to the B_2 phase is shown with bubbles and defects, which persist several degrees below the isotropic–B_2 transition. On cooling from the B_2 phase, the schlieren texture changes into a peculiar stripe texture, figure 3 (*b*), which is typical for the B_7 phase [16, 14].

4.3. *Application of an electric field*

The typical fine stripes accompanying the fan-shaped texture in the B_2 phase, see figures 2 (*a*) and 4 (*b*), disappear under a d.c. electric field of about 0.5 V μm^{-1} and reappear when the field is switched off. In a low frequency a.c. field (5–15 Hz) the extinction is not changed for opposite polarities, and the stripes are absent when the field passes through zero. After the a.c. field is switched off the stripe texture appears within a few seconds. In all cases the extinction position is still directed along the smectic layer normal, but birefringence (colour) changes under the field intensity.

With compounds **4b**, **4c** and **4d**, the texture described above evolves under sufficient a.c field, the changes being significant within several minutes. New wide stripes with different birefringence and behaviour in an electric field start to grow. In the newly appearing area

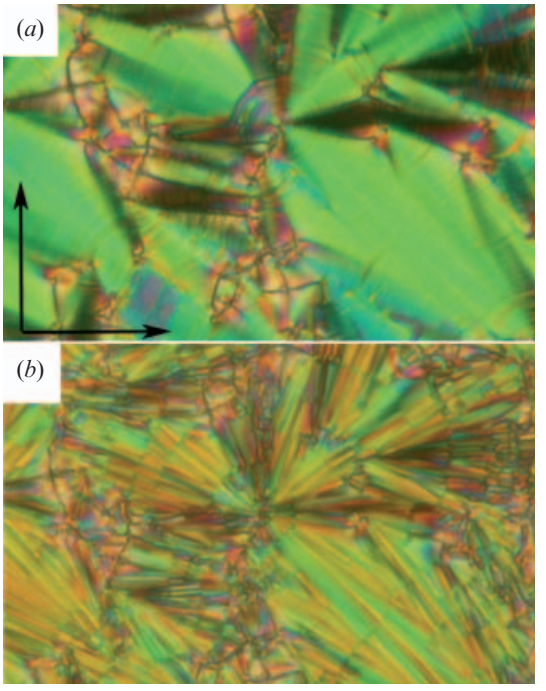

Figure 2. Planar texture of compound **4c** in (*a*) the B_2 phase at $T=182^{\circ}$, (*b*) the B_7 phase at $T=150^{\circ}$C. Width of figures corresponds to 200 µm.

the extinction position rotates from the position of crossed polarizers (in zero field) clockwise or anti-clockwise for the opposite field polarity—red fans and red stripes growing on green fans, see figures 4 (*a*,*c*) for compound **4b**. The rest of the original texture behaves in the electric field the same way as before its application, i.e. the extinction position does not incline under the electric field (green fans in figures 4 (*a*,*c*) for

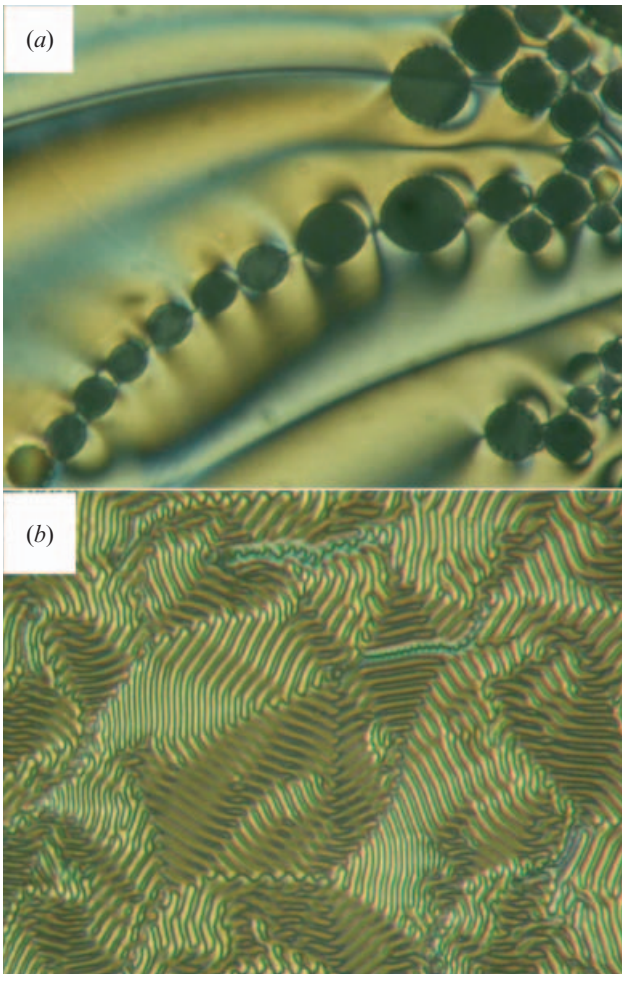

Figure 3. Texture of free-standing film of compound **4b** (*a*) near the isotropic-B_2 phase transition, (*b*) in the B_7 phase. The width of photomicrographs is 150 µm.

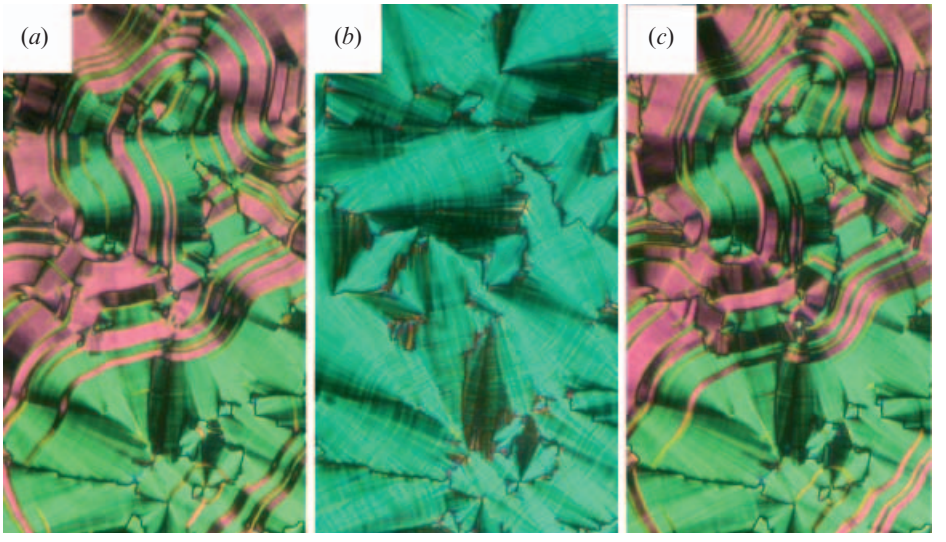

Figure 4. Photomicrographs (width 250 µm) of the planar texture of compound **4b** in the B_2 phase: (*b*) $E=0$; (*a*), (*c*) switching of the same sample area after a.c. field treatment of $20\,V\,\mu m^{-1}$ at 10 Hz for several minutes.

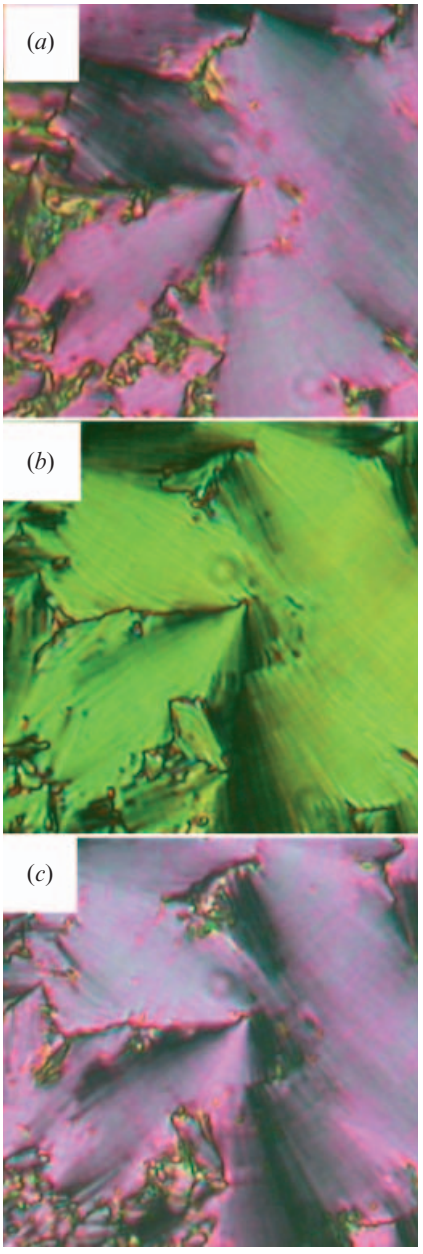

Figure 5. Switching of transformed homochiral domain state of compound **4c**: (*a*) $+20\,V\,\mu m^{-1}$, (*b*) $0\,V\,\mu m^{-1}$, (*c*) $-20\,V\,\mu m^{-1}$. The width of each photomicrograph is 150 µm.

compound **4b**); only the birefringence changes in comparison with the no-field situation.

A further increase of the a.c. field and/or its longer application leads to complete transformation into a new texture, in which the extinction position rotates under the field polarity, and the birefringence differs in the texture in the electric field from the situation without field (figure 5 for compound **4c**). The rotation angle under the electric field with respect to the position of crossed polarizers is estimated as about 22°. The field-induced textures (shown in figures 4 (*a*,*c*) for compound **4b** and figure 5 for compound **4c**) persist even when the field is switched off for a long time. The virgin structure with fine stripes can be reached only by heating to the isotropic phase and subsequently cooling to the B_2 phase.

Antiferroelectric switching has been observed in the B_2 phase of all the studied compounds under a triangular wave field of about $20\,V_{pp}\,\mu m^{-1}$. Two distinct peaks in the polarization reversal current are clearly seen (figure 6). In the B_7 phase no current peak is observed, but below the B_2–B_7 phase transition some electro-optic response can be observed. This response gradually decreases on cooling and fade away within several degrees.

4.4. *Dielectric spectroscopy*

The frequency dependences of complex permittivity, $\varepsilon^*(f)$, show a single relaxation process in the B_2 phase. For most of the compounds this mode vanishes 3–5°C below the B_2–B_7 phase transition; in **4c**, this mode was detected in the whole temperature range of the B_7 phase. A 3-dimensional plot of the imaginary part of ε^* is presented in figures 7 (*a*) and 7 (*b*) for **4b** and **4d**, respectively. The temperature dependences of fitted values of the relaxation frequency f_r and dielectric strength $\Delta\varepsilon$ are shown in figure 8 for compound **4c**. $\Delta\varepsilon$ decreases steeply below the B_2–B_7 phase transition but no anomaly was found in the $f_r(T)$ dependence at this transition; f_r continuously decreases on cooling with no remarkable change.

4.5. *X-ray data*

The X-ray pattern exhibits sharp small angle reflections and a diffuse scattering maximum in a large angle region within both mesophases. This indicates a layered structure with liquid-like molecular packing within the layers. The qualitative character of the X-ray data is very similar for both the B_2 and B_7 phases. From the reflections in the small angle region the layer spacing, *d*, could be determined. The temperature dependence of *d* for compound **4c** is shown in figure 9. The layer spacing decreases on cooling in the B_2 phase and the B_2–B_7 phase transition is manifested as a noticeable anomaly. For the compounds studied, *d* is considerably smaller than calculated molecular length *l*, which proves the tilted arrangement of the molecules. The *l* values were calculated so the tilt angle, Θ, could be roughly estimated as approximately 23°. The calculated value of Θ fits with the angle of rotation of extinction brushes from the crossed position on inducing the homochiral structure (see § 3.3).

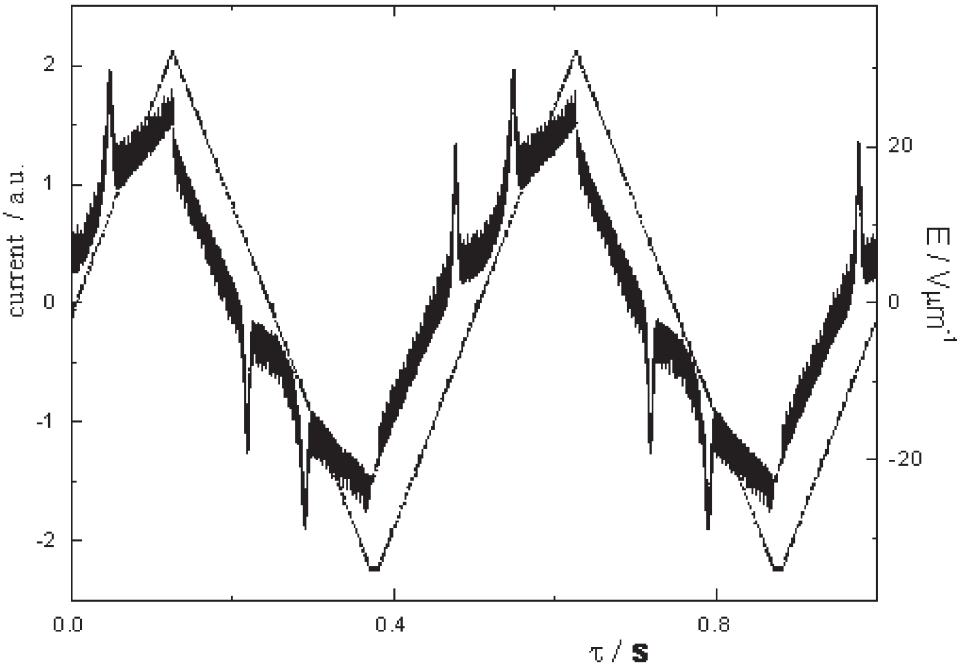

Figure 6. Switching current profile for compound **4c** at $T=175^{\circ}C$.

5. Discussion and conclusions

We have synthesized thermally stable banana-type materials with two mesophases. The high temperature phase is identified as the B_2 phase. In planar geometry this phase exhibits typical fan-shaped texture with fine stripes. The switching current, with two peaks and low $\Delta\varepsilon$ values, confirms the antiferroelectric (AF) character of the observed B_2 phase. Under an electric field the transition to the ferroelectric (FE) state occurs. One can expect no layer chirality change during the transition as long as it remains reversible. When in such a case the extinction direction remains along the layer normal in both field-off AF and field-on FE states, the field-off structure is neither homogeneously chiral (SmC_AP_A) nor simple racemic (SmC_SP_A).

Two models of the AF structure have been proposed, which describe no effective change of optical extinctions position under an electric field. It was first suggested that the structure is composed of mesoscopic chiral SmC_AP_A domains of opposite handedness, which are transformed under the field to the SmC_SP_F structure with opposite tilt in each domain [17]. Then also the overall structure under the field would be effectively anticlinic. The second model [18] proposes a structure composed of racemic SmC_SP_A domains differing in tilt direction, figure 10 (*a*), which are transformed to the SmC_AP_F structure under the field, figure 10 (*b*). If the boundaries between neighbouring field-off domains are parallel to the smectic layers, additional periodicity is created, which effectively increases the symmetry to C_{2v} and the structure exhibits the extinction position along the layer normal. We suppose that this model satisfactorily describes our observation of field switching without change of extinction position parallel to the polarizers. The regular stripe pattern, observed in the planar texture, figures 2 (*a*) and, 4 (*b*), and disappearing under the field, can be attributed to boundaries between the SmC_SP_A domains differing in tilt direction [18]. This model also provides a basis for explanation of observed irreversible changes of planar structure under an a.c. field.

The appearance of broad stripes across the fan-shape texture, after a.c. field treatment for several minutes, can be explained by a change of layer chirality, which is accomplished by rotation of molecules about their long axis. We propose that during a.c. switching the homochiral structure, which grows in broad stripes, predominates over the racemic texture, which remains as the narrow green stripes in figures 4 (*a*,*c*). Changes of layer chirality are shown in figure 10 by horizontal arrows. It may happen that adjacent stripes have opposite chirality and thus opposing rotations of extinction under the field. For a still longer application of the a.c. field (or for higher intensity) the narrow racemic stripes disappear, as well as the broad stripes with opposite chirality, and the whole sample becomes homogeneously chiral; see the scheme in figures 10 (*d*,*e*) that corresponds to the planar texture changes under field in figure 5. Classical switching in the homogeneously chiral structure with opposite rotation of

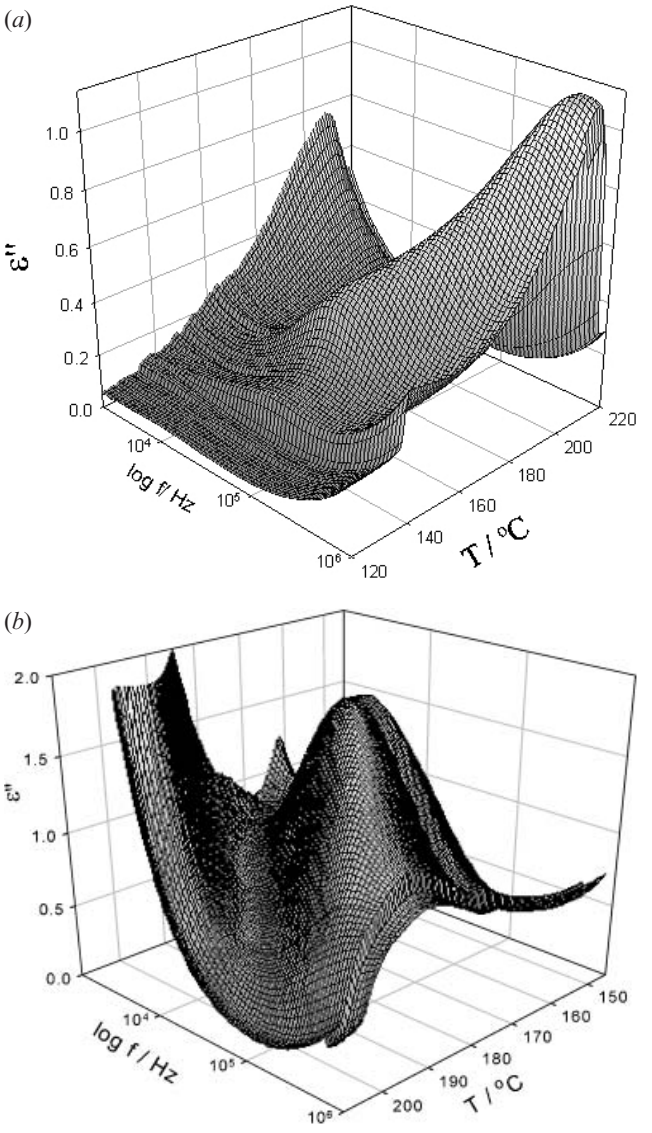

Figure 7. Temperature–frequency plots of the imaginary part of dielectric permittivity taken on cooling from the isotropic phase for (*a*) **4b**, (*b*) **4d**.

extinction in opposite field then takes place. The structure is stable until heating produces the isotropic phase.

Field-induced switching of chirality, or the simultaneous appearance of racemic and chiral structures, have been reported recently [19–21], but for different structures and conditions. In our case the switching of chirality is irreversible and the virgin texture corresponds to the racemic SmC_SP_A phase. We suppose that below the phase transition from the isotropic phase the racemic structure possesses slightly lower energy than the chiral structure, but is realized with many boundaries, which increase the total energy. The switching mediates the change of chirality by rotation of molecules around their long axis and gradually the

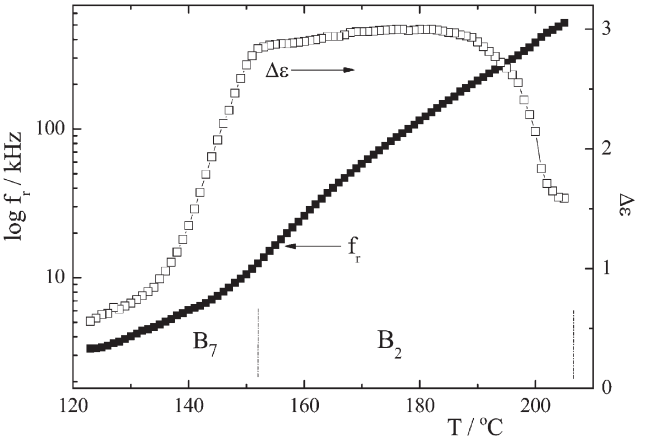

Figure 8. Fitted value of $\Delta\varepsilon$ and log f_r for compound **4c** as functions of temperature.

boundaries are expelled. The resulting homochiral structure might have higher energy, but spontaneous transition to the racemic structure could not be realized without defects, which costs additional energy.

For all the compounds studied a low temperature phase exists below the B_2 phase on cooling. Both observed mesophases exhibit a layered structure. X-ray studies performed on non-oriented samples provided information on layer spacing. From a comparison of these values with calculated values of molecular length, the tilt angle has been determined as about 23°. Recently, on chemically similar compounds with methoxy substitution, the undulation of layers has been confirmed by synchrotron studies [14] for the low temperature phase. So the existence of a B_7-like phase for the compounds presented here could be deduced from similarities of mesomorphic behaviour and textures; mainly, specific features observed in free-standing

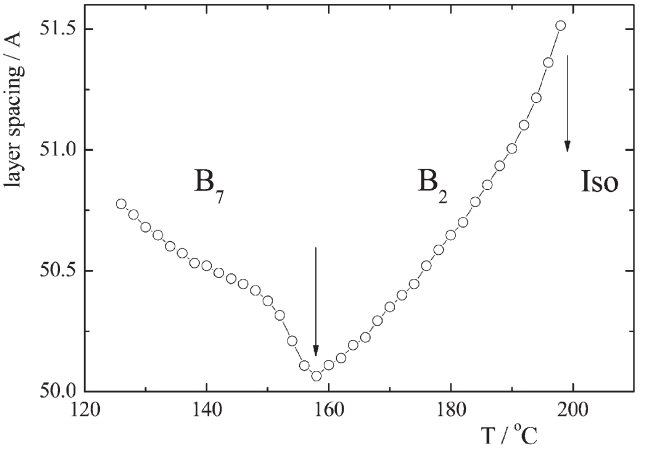

Figure 9. Temperature dependence of the layer spacing for compound **4c**.

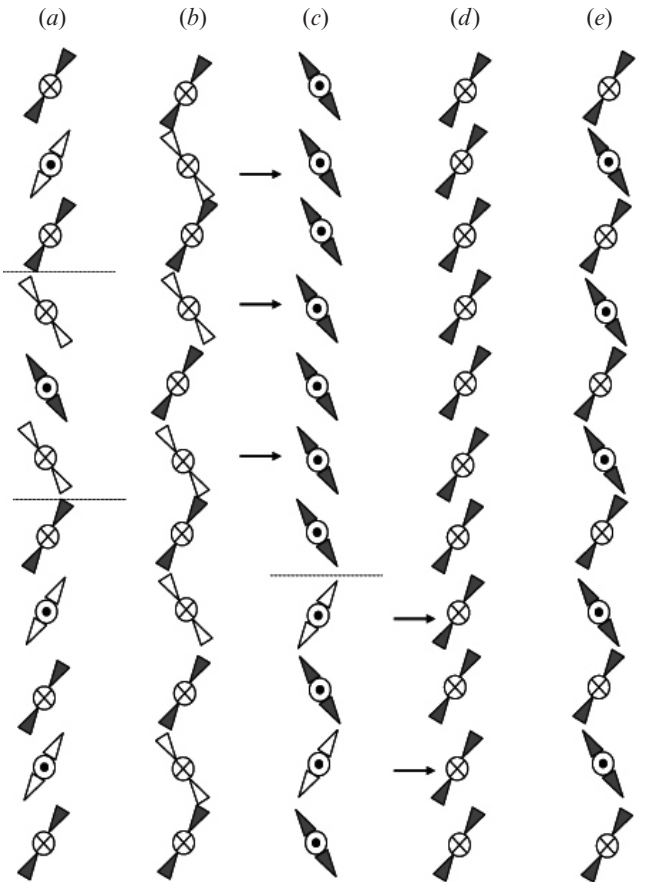

Figure 10. Model of transformation from racemic to homochiral state in relation to chirality switching. Different chiralities are distinguished by black and white colours; layers are packed horizontally. (*a*) Virgin racemic domains for $E=0$, bold dashed lines demark interlayer boundaries; (*b*) switching under d.c. field $E>E_c$, before treatment of the a.c. field; (*c*) and (*d*) describe the situation after application of a low frequency a.c. field $E<-E_c$ and $E>E_c$, respectively. Arrows connect two corresponding states in which the chirality irreversibly changed its sign under application of the a.c. field. (*e*) Resulting homochiral structure without electric field.

films. Nevertheless, the detailed synchrotron analysis is necessary to prove the structure of the low temperature phase presented here.

The presence of terminal double bonds does not significantly influence the mesomorphic properties of the studied series. From these compounds new polymeric materials are under preparation.

Acknowledgements

This work was supported by grant No. 202/05/0431 from the Grant Agency of the Czech Republic.

References

[1] T. Niori, T. Sekine, J. Watanabe, T. Furukawa, H. Takezoe. *J. Mater. Chem.*, **6**, 1231 (1996).
[2] D.R. Link, G. Natale, R. Shao, J.E. Maclennan, N.A. Clark, E. Körblova, D.M. Walba. *Science*, **278**, 1924 (1997).
[3] D.M. Walba, E. Körblova, R. Shao, J.E. Maclennan, D.R. Link, M.A. Glaser, N.A. Clark. *Science*, **288**, 2181 (2000).
[4] G. Pelzl, M.W. Schröder, U. Dunemann, S. Diele, W. Weissflog, C. Jones, D.A. Coleman, N.A. Clark, R. Stannarius, J. Li, B. Das, S. Grande. *J. mater. Chem.*, **14**, 2492 (2004).
[5] H.N. Shreenivasa Murthy, B.K. Sadashiva. *J. mater. Chem.*, **14**, 2813 (2004).
[6] A. Eremin, H. Nadasi, G. Pelzl, S. Diele, H. Kresse, W. Weissflog, S. Grande. *Phys. Chem. chem. Phys.*, **6**, 1290 (2004).
[7] E. Gorecka, D. Pociecha, F. Araoka, D.R. Link, M. Nakata, J. Thisayukta, Y. Takanishi, K. Ishikawa, J. Watanabe, H. Takezoe. *Phys. Rev. E*, **62**, R4524 (2000).
[8] K. Kumazawa, M. Nakata, F. Araoka, Y. Takanishi, K. Ishikawa, J. Watanabe, H. Takezoe. *J. mater. Chem.*, **14**, 157 (2004).
[9] J.P. Bedel, J.C. Rouillon, J.P. Marcerou, M. Laguerre, H.T. Nguyen, M.F. Achard. *Liq. Cryst.*, **27**, 1411 (2000).
[10] G. Dantlgraber, A. Eremin, S. Diele, A. Hauser, H. Kresse, G. Pelzl, C. Tschierske. *Angew. Chem. Int. Ed.*, **41**, 2408 (2002).
[11] D.A. Coleman, J. Fernsler, N. Chattham, M. Nakata, Y. Takanishi, E. Körblova, D.R. Link, R.-F. Shao, W.G. Jang, J.E. Maclennan, O. Mondain-Monval, C. Boyer, W. Weissflog, G. Pelzl, L.-C. Chien, J. Zasadzinski, J. Watanabe, D.M. Walba, H. Takezoe, N.A. Clark. *Science*, **301**, 1204 (2003).
[12] K. Fodor-Csorba, A. Vajda, A. Jakli, C. Slugovc, G. Trimmel, D. Demus, E. Gacs-Baitz, S. Holly, G. Galli. *J. mater. Chem.*, **14**, 2499 (2004).
[13] M. Kašpar, V. Hamplová, V. Novotná, M. Glogarová, P. Vaněk. *J. Mater. Chem.*, **12**, 2221 (2002).
[14] V. Novotná, V. Hamplová, M. Kašpar, M. Glogarová, K. Knížek, S. Diele, G. Pelzl, C. Jones, D. Coleman, N.A. Clark, *Liq. Cryst.* (in the press).
[15] M. Kašpar, M. Glogarová, V. Hamplová, H. Sverenyák, S.A. Pakhomov. *Ferroelectrics*, **148**, 103 (1993).
[16] G. Pelzl, M.W. Schröder, U. Dunemann, S. Diele, W. Weissflog, C. Jones, D.A. Coleman, N.A. Clark, R. Stannarius, J. Li, B. Das, S. Grande. *J. Mater. Chem.*, **14**, 2492 (2004).
[17] C.L. Folcia, J. Ortega, J. Etxebarria. *Liq. Cryst.*, **30**, 1189 (2003).
[18] P. Pyc, J. Mieczkowski, D. Pociecha, E. Gorecka, B. Donnio, D. Guillon. *J. mater. Chem.*, **14**, 2374 (2004).
[19] M.W. Schröder, S. Diele, G. Pelzl, W. Weissflog. *Chem. Phys. phys Chem.*, **5**, 99 (2004).
[20] A. Eremin, S. Diele, G. Pelzl, W. Weissflog. *Phys. Rev. E*, **67**, 020702 (2003).
[21] S. Umadevi, B.K. Sadashiva. *Liq. Cryst.*, **32**, 287 (2005).